Chemistry and Physics of Lipids 218 (2019) 22–33

Contents lists available at ScienceDirect

Chemistry and Physics of Lipids

journal homepage: www.elsevier.com/locate/chemphyslip

Molecular interactions and physico-chemical characterization of quercetin-loaded magnetoliposomes

Sandra Cruz dos Santos[a], Nichole Osti Silva[a], João Batista dos Santos Espinelli Junior[a], Marcelo Augusto Germani Marinho[b], Zeane Vieira Borges[c], Natália Bruzamarello Caon Branco[d], Fabrício Luiz Faita[e], Bruno Meira Soares[a], Ana Paula Horn[b], Alexandre Luís Parize[d], Vânia Rodrigues de Lima[a,*]

[a] Environmental Chemistry and Technology Graduate Program, College of Chemistry and Food Science, Federal University of Rio Grande, Av. Itália km 8, Carreiros Campus, Rio Grande, RS, 96201-900, Brazil
[b] Physiological Science Graduate Program, Biology Department, Federal University of Rio Grande, Av. Itália km 8, Carreiros Campus, Rio Grande, RS, 96201-900, Brazil
[c] Science and Material Engineering Graduate Program, Mechanical Engineering Department, Federal University of Santa Catarina, Trindade Campus, P.O. Box 476, Florianópolis, SC, 88040-900, Brazil
[d] Chemistry Department, Federal University of Santa Catarina, Trindade Campus, P.O. Box 476, Florianópolis, SC, 88040-900, Brazil
[e] College of Physics, Federal University of Rio Grande do Sul, Porto Alegre, RS, 91501-970, Brazil

ARTICLE INFO

Keywords:
Quercetin
Magnetoliposomes
Maghemite
Asolectin
Hyperthermia

ABSTRACT

The bioflavonoid quercetin may prevent magnetoliposomes oxidation, preserving their stability. In this work, the interaction between quercetin and asolectin-based magnetoliposomes was investigated by monitoring the hydration degree, vibrational, rotational and translational mobility parameters of the system as well as its thermodynamic properties. The efficiency of the encapsulation of maghemite magnetic nanoparticles was detected by high resolution-continuum source flame atomic absorption spectrometry (HR-CS FAAS). The magnetic behavior of the system was studied by vibrating sample magnetometry (VSM) technique. The size and surface charge of magnetoliposomes were detected by dynamic light scattering (DLS) and zeta potential (ζ-potential) measurements. The influence of quercetin on the physico-chemical parameters of the magnetoliposomes was evaluated by Fourier transform infrared spectroscopy (FTIR), ^{31}P and ^{1}H nuclear magnetic resonance (NMR) and differential scanning calorimetry (DSC) techniques. In vitro antioxidant and antitumoral assays were also performed for the magnetoliposomes. An insertion of quercetin into magnetoliposomes reduced the efficiency of the encapsulation of maghemite nanoparticles by 11%, suggesting a significant interaction between flavonoid and nanoparticles in a specific region of the system. Quercetin discreetly decreased the saturation magnetization of magnetoliposomes, but did not affect the superparamagnetic behavior of the system. ^{31}P and ^{1}H NMR results showed that quercetin did not alter the inverted hexagonal system phase state but decreased lipid polar head mobility. The flavonoid also seems to reorient the choline group above the bilayer phosphate membrane plane, as indicated by ζ-potential system values. FTIR, NMR and DSC responses showed that quercetin disordered the carbonyl and the methylene regions of the magnetoliposomes. Quercetin, as the nanoparticles, seems to be located in the polar head regions of magnetoliposomes, ordering it and diminishing the lipid intermolecular communication in the membrane carbonyl and non-polar regions. The lipid peroxidation of the magnetoliposomes was prevented 8-fold by the presence of quercetin in the system. Also, the flavonoid was responsible for a 45% reduction in the viability of glioma cells. Location and interactions between quercetin and magnetoliposomes components were discussed in order to be correlated with the results of biological activity, contributing to the design of more stable and efficient magnetoliposomes to be applied as contrast and antitumoral agents.

* Corresponding author at: College of Chemistry and Food Science, Federal University of Rio Grande, Av. Itália, km 8, Carreiros Campus, Rio Grande, RS, 96203-900, Brazil.
E-mail addresses: vrlima23@hotmail.com, vanialima@furg.br (V. Rodrigues de Lima).

https://doi.org/10.1016/j.chemphyslip.2018.11.010
Received 5 May 2018; Received in revised form 30 October 2018; Accepted 30 November 2018
Available online 30 November 2018

1. Introduction

Magnetoliposomes (ML), based on magnetic nanoparticles (MNP) and liposomes (LP), have a versatile structure and permeability under low frequency magnetic fields (Soenen et al., 2009; Ye et al., 2016; Bixner and Reimhult, 2016; Chen et al., 2010; Khaleghi et al., 2016). The magnetic properties attributed to the MNP presence make ML advantageous in theranostic applications and hyperthermia treatment for tumors, as well as a contrast agent (Guo et al., 2015; Babincova et al., 2002; Martins et al., 2014). Furthermore, LP are one of the most successful carriers for co-delivery, enabling MNP biocompatibility and reducing its toxicity (Caddeo et al., 2017; Barenholz, 2001). LP are also versatile, due to their ability to encapsulate both hydrophobic and hydrophilic drugs. Many recently studied ML are composed of synthetic phospholipids (Ding et al., 2012; Xia et al., 2014; Floris et al., 2014). However, the use of natural phospholipids is available in larger scale at relatively low costs compared to synthetic phospholipids and also shows lower toxicity (van Hoogevest and Wendel, 2014; Sercombe et al., 2015a). Natural-sourced phospholipids, such as soybean phosphatidylcholine loaded with magnetic nanoparticles, have been highlighted as a new drug delivery system (Spera et al., 2014). They show high biodegradability, biocompatibility and non-immunogenicity, since their structure and organization are similar to human biological membranes (Torchilin, 2005; Edwards and Baeumner, 2006).

The stability of ML is still a challenge for their design, since they are susceptible to Fe^{2+} and Fe^{3+}-induced membrane peroxidation (Kiwada et al., 1986; Fagali and Catala, 2009; Gutteridge, 1995). In this context, quercetin (3,3',4',5'-7-penta-hydroxy flavone – QC, Fig. 1) is a natural-sourced bioflavonoid with well-established antioxidant properties which can prevent ML oxidation. It is known that QC-loaded LP display strong 2,2-diphenyl-1-picrylhydrazyl (DPPH) scavenging and lipid peroxidation inhibition capacity (Gabrielska et al., 2006; Huang et al., 2017). Antioxidant properties of QC-induced LP are also related to the metal-chelating properties of flavonoids, as well as to their location and the ordering effect of QC/prooxidative compound complexes in the membrane (Gabrielska et al., 2006).

QC has the ability to interact with membranes due to either the hydrophobic or the polar head domains (Movileanu et al., 2000). Since the flavonoid shows important anti-cancer activities (Chakraborty et al., 2012; Wong and Chiu, 2011), liposomal QC is effective as a tumor-targeted drug carrier (Hirpara et al., 2009; Takagi et al., 1998). Furthermore, the encapsulation of QC into the systems of lipid bilayers may reduce drug disadvantages such as their poor solubility in water, short biological half-life and low oral bioavailability (Hadrich et al., 2016; Hollman et al., 1996).

Despite the extensive knowledge concerning QC interaction with LP, there is little information concerning QC behavior in ML. Indeed, it is reported that QC-conjugated MNP were promising as anticancer agents for targeted drug delivery (Kumar et al., 2014; Barreto et al., 2011; Akal et al., 2016). Thus, considering the lower peroxidation susceptibility of ML and the promising antitumoral activity of the QC-MNP association, it is important to characterize the ML-QC system in the context of molecular interactions and antioxidant/antitumoral activities. This can contribute to a suitable design of ML systems.

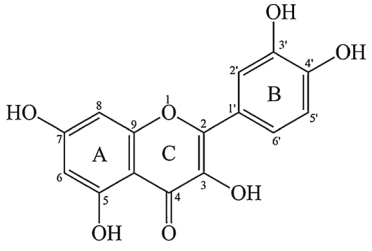

Fig. 1. Structure of quercetin.

Actually, the integrity and efficiency of drug delivery systems are governed by their physico-chemical properties, such as charge, particle size, mobility, state-of-phase, order degree and vibrational, rotational and translational rates. These ones are influenced by molecular interactions (Sercombe et al., 2015b). In this work, soybean asolectin (ASO)/maghemite (γ-Fe_2O_3) MNP -based ML containing QC (abbreviated as ML_QC) were prepared and had their physico-chemical properties and molecular interactions investigated and correlated with in vitro antioxidant and antitumoral activities.

Natural-sourced ASO contains approximately 25% egg yolk L-α-phosphatidylcholine (PC), 25% cephalin (egg yolk L-α-phosphatidylethanolamine – PE), 25% phosphatidylinositol and small amounts of other polar phospholipids from soybeans (Johns et al., 2015). Thus, properties of ML_QC such as encapsulation efficiency, magnetization, size, surface charge and orientation, morphology, hydration degree, phase state, order degree and thermodynamic parameters were characterized by high resolution-continuum source flame atomic absorption spectrometry (HR-CS FAAS),vibrating sample magnetometry (VSM), dynamic light scattering (DLS), zeta potential (ζ-potential), Fourier transform infrared spectroscopy (FTIR), ^{31}P and ^{1}H nuclear magnetic resonance (^{31}P NMR and ^{1}H NMR) and differential scanning calorimetry (DSC). Results described in this work will contribute to the design of more stable and efficient ASO-based ML_QC systems being used as antitumoral agents.

2. Materials and methods

2.1. Materials

ASO (containing 25% soy PC), maghemite MNP (γ-Fe_2O_3 50 nm diameter, at maximum), tricine, magnesium chloride, chloroform, QC, deuterated water/sodium3-(trimethylsilyl)-[2,2,3,3-2H4]-1-propionate (TSP, 0.05%),3-(4,5-dimethylthiazol-2-yl)-2,5-diphenyltetrazolium bromide (MTT) and thiobarbituric acid were purchased from Sigma-Aldrich (Missouri, USA). Hydrogen peroxide, phosphate buffer (KH_2PO_4) and trichloroacetic acid (TCA) were bought from Synth (São Paulo, Brazil). Fetal bovine serum and Dulbecco's modified Eagle's medium (DMEM) were purchased from Invitrogen Co. (Carlsbad, USA). Lipids were used without further purification and all the other chemicals were of analytical grade. Ultrapure water was used for the preparation of all reagents, and reference solutions were purified by a Milli-Q system model Direct-Q UV3, Millipore (New Jersey, USA). Concentrated HNO_3 (65%) and HCl (35%) obtained from Merck (Darmstadt, Germany) were distilled in a sub-boiling system model DuoPur (Milan, Italy).

2.2. ML preparation

ML_QC and pure ML were prepared by a modified reverse-phase evaporation method (Mertins et al., 2005; Szoka and Papahadjopoulos, 1978). Briefly, ASO (100 mg mL^{-1}) was dissolved in chloroform and methyl alcohol (3:1,v/v). In this solution, 20 μL of a solution containing maghemite MNP (0.14 mg mL^{-1}) was added to pH 7.4 buffer (tricine10 mmol L^{-1} and $MgCl_2$ 2.5 mmol L^{-1}). Thus, the total MNP/lipid ratio was 0.0014 (w/w) (Qiu et al., 2012). Then, the mixture was homogenized for 3 min in a bath sonicator, yielding an opalescent dispersion of reverse micelles. Solvents were evaporated in a rotatory evaporator at 33 °C under vacuum to generate a viscous organogel. The organogel was re-dispersed in chloroform and the solvent was rotaevaporated one more time. The organogel was then hydrated with a pH 7.4 buffer (tricine 10 mmol L^{-1} and $MgCl_2$ 2.5 mmol L^{-1}). QC was previously solubilized in methyl alcohol and added into the co-solubilization step (total QC to ASO ratio was 0.0015 w/w; equivalent to a QC concentration of 500 μmol L^{-1}). QC concentration choice was based on studies performed by Jeon et al. (2015).

All samples were sonicated for 15 min to obtain liposomes

homogeneity. Then, they were centrifuged at 20 °C, 1000 × *g* for 15 min, to separate unincorporated MNP and QC-loaded ML in the supernatant (Kulshrestha et al., 2012). Furthermore, the prepared ML and ML_QC were preserved at 4 °C before being analyzed by DLS, ζ-potential, HATR-FTIR, ^{31}P NMR, ^{1}H NMR spin-lattice relaxation times (T_1) and DSC. For these measurements, two liposomes control samples were also tested, one in the presence of quercetin (LP_QC) and the other in the absence of quercetin QC (LP).

2.3. MNP encapsulation efficiency in ML

The determination of MNP and encapsulation efficiency (EE%) in ML (ASO 100 mg mL^{-1}; MNP added concentration 0.14 mg mL^{-1}), in the absence and in the presence of QC (total QC to ASO ratio was 0.0015 w/w; equivalent to a QC concentration of 500 μmol L^{-1}), was determined by HR-CS FAAS, which was carried out in a high-resolution continuum source atomic absorption spectrometer model ContrAA 700Analytik Jena (Berlin, Germany). A Xe short-arc lamp GLE (Berlin, Germany) operating in "hot-spot" mode was used as a radiation source. A linear CCD array detector with 588 pixels (200 used for analytical purposes and the remaining for internal functions) was also used. The flame composition was operated with an acetylene flow rate of 1.8 L min^{-1} and an air flow rate of 60 L min^{-1}. The measurements were carried out using the most sensitive analytical line for iron 248.327 nm.

The iron measurements by HR-CS FAAS were performed after microwave-assisted acid digestion (MW-AD). For this sample preparation method, a microwave sample preparation system model MARSXpress, CEM Corporation (North Rhine-Westphalia, Germany) was used. ML supernatant samples (about 200 mg) were transferred to the PTFE vessels with 6 mL of concentrated HNO_3. The vessels were placed inside the microwave oven, and the heating program was as follows: *i*) 960 W (with a ramp of 15 min); *ii*) 960 W for 15 min and *iii*) 0 W for 20 min (cooling step). After digestion, the pressure of each vessel was carefully released. The digests were diluted with up to 30 mL of ultrapure water for subsequent determination of Fe by HR-CS FAAS.

The EE% of MNP in the ML was calculated as presented below:

$$EE\,(\%) = [MNP]_s/[MNP]_{add} \times 100 \quad (1)$$

Where $[MNP]_s$ is the concentration the MNP found in the supernatant after centrifugation steep and $[MNP]_{add}$ is the concentration of the MNP added in the preparation of the ML. The limit of detection (LOD) was calculated as three times the standard deviation of ten measurements of blanks ($n = 10$) divided by the slope of the calibration curve. The accuracy of this method was determined by a recovery assay after a spike of 0.17 mg L^{-1} of Fe.

2.4. Magnetization assays

The magnetic behavior and properties of the ML were investigated by magnetization versus magnetic field measurements performed using a MicroSense EV9 vibrating sample magnetometer (VSM) model MicroSense LLC (Massachusetts, USA). The applied magnetic field range was −5000 to +5000 Oersted (Oe). All measurements were performed at 310 K to simulate body temperature and study the magnetization response in this specific condition. The magnetization was measured along the applied field direction. The sample analyses were ML (ASO 100 mg mL^{-1}; an MNP added concentration of0.14 mg mL^{-1}), both in the absence and in the presence of QC (sample ML_QC, total QC to ASO ratio was 0.0015 w/w; equivalent to a QC concentration of 500 μmol L^{-1}).

2.5. Physico-chemical characterization

For physico-chemical characterization, analyses of the ML (ASO 100 mg mL^{-1}; MNP added concentration 0.14 mg mL^{-1}), in the absence and in presence of QC (sample ML_QC, total QC to ASO ratio was 0.0015 w/w; equivalent to a QC concentration of 500 μmol L^{-1}) were shown as the mean of triplicates from three independent experiments. As cited before, control measurements were performed with LP (ASO 100 mg mL^{-1}) and LP_QC (total QC to ASO ratio was 0.0015 w/w; equivalent to a QC concentration of 500 μmol L^{-1}).

2.5.1. Size measurements

The mean hydrodynamic radius of the ML, ML_QC, as well as control-LP and LP_QC was determined using a Dynamic Light Scattering instrument, Zetasizer Malvern UK-NanoZS instrument (Malvern Instruments Ltd., Worcestershire, England). Intensity correlation functions were measured at a scattering angle of θ = 173°, using a wavelength of 488 nm. To determine size distribution, samples were diluted 40 times with ultrapure water and analyzed in an optical grade polystyrene cuvette at 25 °C. The z-averaged and intensity-weighted hydrodynamic diameters were based on three measurements, each one based on 14 scans. All reported hydrodynamic radii were calculated using Stokes-Einstein equation:

$$r_h = kT/(6\pi\eta D) \quad (2)$$

Where k is Boltzmann's constant, T is the temperature and η is the solvent viscosity, D is the diffusion constant and r_h is the hydrodynamic radius of the spherical particle.

2.5.2. ζ-potential measurements

The surface charge of the ML, ML_QC, as well as the control-LP and LP_QC was measured by the Electrophoretic Light Scattering (ELS) mode of the same instrument used for particle size distribution. Samples were measured at 25 °C, with a laser scattering angle of 173° in the cell, with the following specifications: a dispersion medium viscosity of 0.894 m P as and a refractive index of 1.33. The laser power and electric field were controlled at 60 mW and 25 V cm^{-1}, respectively. All samples were diluted 40 times with ultrapure water.

2.5.3. HATR-FTIR measurements

HATR-FTIR experiments were performed at 25 °C using Shimadzu IR Prestige-21 equipment (Kyoto, Japan). The ML, ML_QC, as well as control-LP and LP_QC were deposited on a ZnSe crystal support and immersed into ultrapure water. Interferograms were averaged for 40 scans, recorded in a frequency range from 400 to 4000 cm^{-1}, with a resolution of 2 cm^{-1}. The obtained spectra were analyzed by Shimatzu IR solution software 1.5. Frequency value shifts as well changes in the bandwidth of ASO vibrational bands were analyzed. Bandwidths were measured relative to a straight baseline at ¾ (75%) peak height position (Toyran and Severcan, 2007).

2.5.4. NMR assays

^{31}P NMR measurements of the ML, ML_QC, as well as control-LP and LP_QC were performed at 161 MHz using a Bruker DPW 400 NMR spectrometer. The recycling time was 4 s, acquisition time 0.5111808 s, pulse 15.05 μs and delay 0.2 s; 2048 scans were accumulated for each sample. The width measurements of the lines of the P NMR spectra were obtained at 3/4 the phosphorus peak (Niederberger and Seelig, 1976). ^{1}H spin-lattice relaxation times (T_1) were measured with the same NMR equipment for all systems, using the inversion-recovery pulse sequence (π-t-π/2 acquisition) at 25 °C. Time delays ranged from 0.4 to 12.8 s (de Lima et al., 2010). The T_1 values and relative intensities were obtained by fitting the exponential data to the NUTS code.

For both NMR assays, the chemical shifts were referenced to TSP signal at 0 ppm. Deuterated water was used as an external reference (the samples were dispersed in a water/deuterated water solution, 70:30, v/v).

2.5.5. DSC measurements

DSC assays were performed with Shimadzu DSC-60 equipment (Tokyo, Japan). For the ML, ML_QC, as well as the control-LP and

LP_QC, the heating rate was set to 5 °C min^{-1} at a temperature range from −45 to 5 °C, under nitrogen flow (50/50 mL min^{-1}) (Lynch and Steponkus, 1989; Ulrich et al., 1994). An empty aluminum pan was used as a reference (Zhao et al. (2007a)). The enthalpy variation (ΔH) was obtained by integrating the area under the DSC peak with the TA 60WS software.

2.6. Lipid peroxidation assays

ML and ML_QC basal lipid peroxidation (produced by atmosphere reactive species) were evaluated by thiobarbituric acid reactive substance (TBARS) quantification (Bird and Draper, 1984). For this, samples containing 12.50 mg mL^{-1} ASO and showing the same lipid-to-MNP and lipid-to-QC ratio were incubated at 37 °C for 30 min, and 0.15 mg mL^{-1} trichloroacetic acid and 0.00375 mg mL^{-1} thiobarbituric acid were added. After incubation at 100 °C, a malondialdehyde-thiobarbituric acid adduct was detected by ultraviolet-visible (UV–vis) spectroscopy (at 535 nm). Control assays were performed in the presence of LP and LP_QC, as well as without the drug-delivery systems. Lipid peroxidation was expressed as µmol TBARS mg^{-1} lipid.

Percentage of lipid peroxidation was calculated as follows:

$$\text{Lipid Peroxidation (\%)} = \frac{A_Q - A_F}{A_F} \times 100 \quad (3)$$

Where A_Q and A_F correspond to the absorbance (at 535 nm) of the QC-loaded and QC-free systems, respectively. Statistical data analyses were performed using one-way analysis of variance (ANOVA) followed by Dunnett's.

2.7. Cell culture

For cell viability experiments (described in Section 2.7), rat glioblastoma cell line C6 was obtained from the American Type Culture Collection (Maryland, USA). The cell line was cultivated in Dulbecco's Modified Eagle's medium (DMEM) low glucose (Gibco, USA), supplemented with 10% fetal bovine serum (FBS) (Invitrogen, Brazil) and 100 UL^{-1} gentamicin and 2.5 mg mL^{-1} Fungizone® (Gibco, USA). Cells were maintained until the 30th passage in an incubator with an atmosphere of 5% CO_2 at 37 °C. To perform the experiments, C6 rat glioma cells (1×10^4 cells per well) were subcultured on 96-well tissue culture plates for 24 h to adhere and reach subconfluence. Cells were exposed to different treatments for 24 h. Control measurements were performed with MNP (0.14 mg mL^{-1} of maghemite MNP dispersed in ultrapure water), LP (ASO 100 mg mL^{-1}) and LP_QC (total QC to ASO ratio was 0.0015 w/w; equivalent to a QC concentration of 500 µmol L^{-1}, see Section 2.2).

2.8. Cell viability assay

The viability of cells exposed to ML and ML-QC was evaluated by a MTT (3-(4,5-dimethylthiazol-2-yl)-2,5-diphenyltetrazolium bromide) assay, which aims to estimate the viability through cellular mitochondrial metabolism. This assay is based on the reduction of tetrazolium salt to formazan in the respiratory chain of the mitochondria. The reduction reaction only occurs in metabolically intact cells. Thus, the number of viable cells is proportional to the generation of formazan (da Silveira et al., 2013). After 24 h of treatment (see Section 2.6), 50 µL of the MTT solution (stock solution of 5 mg mL^{-1}) were added to each well, and cells were then incubated for 2 h at 37 °C. Quantification was performed by spectrophotometry on an ELISA reader at 490 nm, and the results were expressed as a percentage of viable cells in relation to the control. All experiments were done in triplicate, and results were shown as the mean of triplicates from three independent experiments. A one-way analysis of variance (ANOVA), followed by the Tukey-Kramer post-hoc test for multiple comparisons, was performed. Differences among mean values were considered significant when $p < 0.05$.

Table 1
Total MNP concentration and encapsulation efficiency (EE%) in magnetoliposomes (ML) and QC-loaded magnetoliposomes (ML_QC).

	[MNP], mg mL^{-1}	EE%
ML_QC	0.101 ± 0.001	43
ML	0.116 ± 0.006	58

3. Results and discussion

3.1. Total MNP concentration and EE% in ML

Total MNP concentration and EE% in the ML were determined by HR-CS FAAS in the absence and presence of QC. These data are reported in Table 1.

MNP concentration values showed good accuracy, with a recovery of 103%, with relative standard deviation (RSDs) lower than 9% and a LOD of 0.025 mg mL^{-1}. The initial MNP concentration in maghemite was 0.14 mg mL^{-1}. Around 0.101 mg mL^{-1} of MNP was loaded into ML, the equivalent of an EE% of 58%.

Previous research showed an EE% of magnetic MNP oxide in the soy PC of 78.10% ± 0.24 (Gharib et al., 2014). The EE% of iron MNP in methotrexate modified thermo-sensitive ML (MNP/lipid ratio of 0.33 w/w) prepared by thin film dispersion method was 87.6% (Guo et al., 2018). Liposomal lipid content or the type of preparation method used may influence the difference between experimental results found on this study and those reported in literature (Lichtenberg and Barenholz, 1988). Indeed, Shubra et al. reported the mass ratio as well as the volume ratio between MNP and the carrier components as variables which affects model drug encapsulation efficiency in PLGA-MNP nanoparticles (Shubhra et al., 2014).

The insertion of QC into ML reduced the MNP EE% by around 15%. Zafar et al. (2014) pointed that the competition between a drug and water molecules for a carrier specific region occurs, evolving electrostatic and non-covalent interactions required for the carrier drug inclusion. This work used hydrophilic carrier and drug models. In our work, dipolar interactions between the lipid polar region and quercetin hydroxyl groups, as well as hydrophobic interactions between the carrier and the flavonoid may favor the MNP diffusion for the external aqueous medium. A correlation between EE% and vesicular size will be discussed in the Section 3.3.

3.2. ML magnetic properties

The magnetic behavior of the maghemite powder (γ-Fe_2O_3 as purchased) and ML was investigated in the solid state and aqueous dispersion, respectively. Fig. 2 shows field dependent magnetization *per*

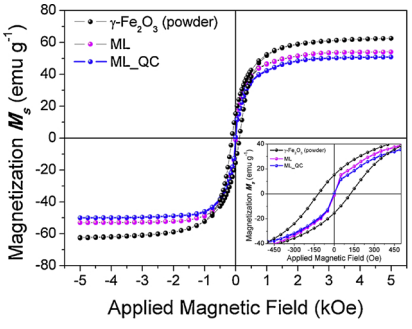

Fig. 2. Magnetic behavior of the maghemite powder (γ-Fe_2O_3), magnetoliposomes without (ML) and with quercetin (ML_QC), at 37 °C. The concentration of the ASO was 100 mg mL^{-1} and total QC to ASO ratio was 0.0015 w/w; equivalent to a QC concentration of 500 µmol L^{-1}. The systems were prepared by modified reverse-phase evaporation method.

mass (*M* vs. *H*) curves. It is important to note that data were recorded at 310 K to simulate the body temperature. The saturation magnetization (*Ms*) value for γ-Fe_2O_3 was 63.3(2) emu g^{-1}, and this result is in accordance with literature (da Silva et al., 2017).

A hysteresis with low coercivity and remanence was observed for maghemite powder, and a superparamagnetic behavior was present for the magnetoliposomes samples (ML and ML_QC – see the inset in Fig. 2). These distinct behaviors can be explained by the presence and/or absence of magnetic interactions/coupling between the superparamagnetic iron oxide nanoparticles (SPIONs). Thus, in the powder, this interaction is promoted due to very low distance of the SPIONs. Conversely, when the SPIONs are incorporated/encapsulated into the liposomes, this distance is significantly increased and the magnetic coupling does not occur. Moreover, both magnetoliposomes samples (ML and ML_QC) show superparamagnetic character, i.e. zero magnetization when the applied magnetic field is removed. This behavior is important for biomedical applications in order to prevent aggregation and enable rapid dispersal in the absence of a magnetic field (Hardiansyah et al., 2017). A reduction in *Ms* by approximately 15% and 17% was observed for the ML (53.7(2) emu g^{-1}) and ML_QC (52.5(1) emu g^{-1}), respectively, when considering the *Ms* from maghemite powder. This reduction in magnetization was expected due to the presence of polymer, organic molecules or surfactant on the surface of SPIONs, which may decrease the *Ms* due to a related increase in the magnetic anisotropy energy constant, and a pinning of the surface spins or quenches the surface magnetic moments (Dresco et al., 1999; Berkowitz et al., 1980). In this context, the *Ms* is 2.2% lower for the ML_QC sample than for the ML sample, which could be due to the addition of the quercetin molecules, which can also interact with the surface of the SPIONs and decrease the magnetization. Finally, the magnetoliposomes *Ms* remain in a sensitive range for magnets exposure (i.e., neodymium-based magnets) to external fields, allowing it to biomedical applications (Ding et al., 2012).

3.3. Systems size and ζ-potential measurements

The size related to ML, ML_QC, and the controls LP and LP_QC (see Section 2.5) are listed in Table 2. Table 2 shows that ML_QC is 63 nm larger than ML. Compared to the QC effect in the size of LP, QC induced an increase in the system size 1.6 times higher in LP than in ML. The higher QC-induced increase in the size of LP is related to the broad transverse flavonoid distribution, which could expand the volume of the LP (Huang et al., 2017). It is known that complexes of iron/flavonoids interact to and connect a pair of bilayers (Tarahovsky et al., 2012), compacting them and maybe diminishing ML size, compared to LP. A proportional correlation between the particle size and the EE% is reported in the literature (Zhao et al., 2007b).Considering the QC effect in LP and in ML, it is important to know that a reduction in the particle size diminishes the length of MNP diffusional pathways from the carrier to the aqueous medium, allowing diffusion and reducing EE% (Budhian et al., 2007). This may reinforce the observations concerning QC and MNP interaction (see Section 3.1). Thus, it is possible that, in ML, complexes of MNP/QC were formed and the remaining free-MNP diffused from membrane to aqueous medium, reducing its EE%.

Magnetic liposomes samples showed a wide range of mean hydrodynamic diameters depending on composition and methods of preparation (Pradhan et al., 2007). The use of different methods of preparation provides different sizes of ML. Pradhan et al. (2007) prepared ML encapsulating lauric-acid-coated water-based manganese ferrite magnetic fluid with different molar ratios of egg-PC and cholesterol by two different methods: thin film hydration (TFH) and double emulsion (DE). The smallest mean hydrodynamic diameter (171.6 nm) was found by the TFH method. For the system prepared by DE method, the size found was twice as large as the that obtained by THF (Pradhan et al., 2007). ML could be mostly prepared by the hydration of a thin lipid film to obtain a swollen lamellar phase in an excess aqueous medium, which can generate different vesicular sizes in function of the type of the sequential mechanical lipids dispersing. High-energy sonication or extrusion through calibrated membrane filters yield unilamellar magnetoliposomes of a rather narrow size distribution and average diameters typically in the 100 to 400 nm range (Marie et al., 2013). Another widely used method is reverse-phase evaporation from a biphasic mix of lipids in diethyl ether solution and aqueous colloidal iron oxide in a saline buffer (Marie et al., 2013).

ML_QC showed no statistically significant difference in the PDI values ($p > 0.05$) compared to the controls. Thus, QC did not influence the distribution size of particles in ML or LP. The distribution found seems to be influenced by the preparation method (Pradhan et al., 2007).

The ζ-potential values of all systems were negative and lower than −30 mV, indicating stable ASO-based colloidal systems, acceptable to be used in lipid formulations. Since the LP negative charge (ζ-potential of −67.9 ± 1.42 mV, Table 2) is due to a significant ASO phosphatidylinositol content (Honary and Zahir, 2013; Ohki et al., 2010), the insertion of negative charged MNP in the system enhanced the ζ-potential in approximately 3 mV (ML, −71.5 ± 1.33 mV). However, the insertion of QC in ML systems (corresponding to ML_QC system, −68.5 ± 1.72 mV) promoted a shift toward a more positive ζ-potential value, very similar to those related to LP and LP_QC. This may be due to the probable complex QC/MNP and to the diffusion of MNP toward the aqueous medium, both commented before. Considering the effect of group orientation in ζ-potential value of different systems (Pradhan et al., 2007; Makino et al., 1991; Jangde and Singh, 2016), it is also possible that, in ML systems, the insertion of MNP reorients the ML choline below the phosphate group plane, promoting a more negative surface charge. Considering the ML_QC system, the complex QC/MNP may orient the choline group above the phosphate group, promoting a more positive ζ-potential.

The effect of the flavonoid in LP ζ-potential value was 50% lower compared to ML, showing that ML surface charge is more sensitive to the effects of QC. This reinforces an effect of both QC and MNP interaction in the lipid polar head of ML. Indeed, it was yet observed a strong electrostatic interaction between QC and magnetite protonation of the surface groups via carboxyl molecules and the presence of anionic ions from the drug molecules which were responsible for a considerable positive surface charge of 6.14 mV (Kumar et al., 2014).

3.4. QC location and influence on specific regions of ML

QC location and influence on the behavior of specific regions of ML

Table 2
QC influence on the dynamic mean diameter (< D >), ζ-potential and polydispersity index (PDI) of ML and LP.

Formulation	< D > (nm)	Δ	ζ-potential (mV)	Δ	PDI
ML_QC	208.62 ± 13.34	63.0 nm[a]	−68.5 ± 1.72	3.0 mV[a]	0.461 ± 0.078
ML	145.62 ± 14.29		−71.5 ± 1.33		0.471 ± 0.017
LP_QC	243.53 ± 6.73	100.7 nm[b]	−66.3 ± 0.49	1.6 mV[b]	0.461 ± 0.004
LP	142.83 ± 0.80		−67.9 ± 1.42		0.465 ± 0.029

The variations (Δ) were calculated about the difference between [a]QC-loaded magnetoliposomes (ML_QC) and magnetoliposomes (ML) and [b]QC-loaded liposomes (LP_QC) and liposomes (LP). The values are shown as the mean ± standard deviation for each group ($n = 3$).

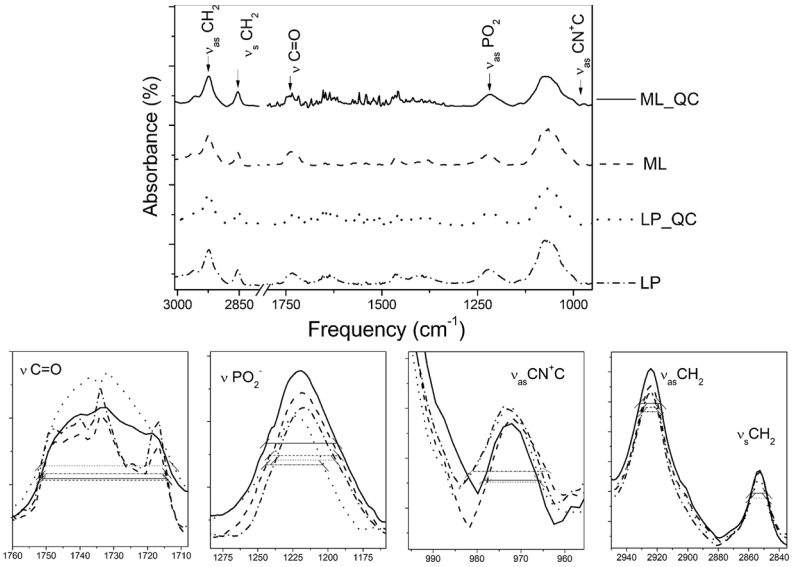

Fig. 3. HATR-FTIR spectra of QC-loaded magnetoliposomes (ML_QC) and magnetoliposomes (ML), QC-loaded liposomes (LP_QC) and liposomes (LP). The total QC to ASO ratio was 0.0015 w/w; equivalent to a QC concentration of 500 μmol L^{-1}, and the concentration of the ASO was 100 mg mL^{-1}. Interferograms were obtained from the average of 40 scans, with a resolution of 2 cm^{-1}, in a frequency range of 400-4000 cm^{-1}.

were investigated by HATR-FTIR, ^{31}P NMR, ^{1}H NMR spin-lattice relaxation times (T_1), DSC, DLS and ζ-potential. As previously cited, results were also compared with the control LP.

The HATR-FTIR spectra of ML and ML_QC and LP_QC and LP-controls are shown in Fig. 3. QC-induced frequency and bandwidth shifts of specific lipid group axial stretching vibrations are reported in Table 3. These stretching vibrations (and their related lipid group) are described as follows: choline antisymmetric stretching (ν_{as} CN^+C), phosphate antisymmetric stretching (ν_{as} PO_2^-), carbonyl stretching mode (ν C═O) and symmetric and antisymmetric stretching of the methylene of acyl chains (ν_s CH_2 and ν_{as} CH_2, respectively). The obtained results were analyzed according to the QC effect in each lipid region and complemented by NMR and DSC studies.

The QC insertion into ML did not affect the frequency values of any ASO group. This indicates that QC had no influence on the number of hydrogen-bounded water molecules around the ML lipid head and carbonyl regions. Also, the flavonoid has no affect in the trans-gauche isomerization of hydrophobic lipid methylene groups. These effects are detailed and discussed as follows.

Table 3
HATR-FTIR frequency values and bandwidth of specific lipid groups related to QC-loaded magnetoliposomes (ML_QC), magnetoliposomes (ML), QC-loaded liposomes (LP_QC) and liposomes (LP).

	ML_QC	ML	Δ[a]	LP_QC	LP	Δ[b]
Frequency (cm^{-1})						
ν_{as} CH_2	2924.72	2924.72	–	2924.72	2924.72	–
ν_s CH_2	2852.72	2852.72	–	2852.72	2852.72	–
ν C═O	1734.01	1734.01	–	1734.01	1734.01	–
ν_{as} PO_2^-	1219.01	1219.01	–	1222.87	1217.08	5.79
ν_{as} CN^+C	972.12	972.12	–	972.12	974.05	1.93
Bandwidth at ¾ peak position (cm^{-1})						
ν_{as} CH_2	6.44	6.44	–	6.44	6.44	–
ν_s CH_2	6.44	6.44	–	6.44	6.44	–
ν C═O	10.00	6.44	3.56	7.77	4.44	3.33
ν_s PO_2^-	11.67	11.11	0.56	8.88	10.55	1.67
ν_{as} CN^+C	2.86	2.86	–	3.54	3.54	–

The variations (Δ) were calculated based on the difference between [a]QC-loaded magnetoliposomes (ML_QC) and magnetoliposomes (ML) and [b]QC-loaded liposomes (LP_QC) and liposomes (LP). The bandwidth values were calculated at 75% of the peak height (dos Santos et al., 2018).

3.4.1. QC effects in ML polar head groups

Changes in HATR-FTIR frequency and bandwidth of stretching vibrations related to choline ASO groups (ν_{as} CN^+C) may be observed when water molecules intercalate between the choline and phosphate regions. Dipole interactions between water molecules and choline are affected by choline conformation changes after to interact with an exogenous molecule (Grdadolnik et al., 1991; Manrique-Moreno et al., 2011a).

The QC insertion into ML did not affect the frequency and bandwidth of $\nu_{as}CN^+C$ peak. This indicates that QC had no influence on the vibrational motions and dipolar interactions related to the ML choline group (Chen and Tripp, 2008). The same behavior was observed for LP_QC, when compared to LP. Comparing ML and LP HATR-FTIR values, one can see that the insertion of MNP into liposomes does not affect significantly lipid choline interactions with water molecules.

To obtain more information about the ML_QC choline behavior, the rotational motion of the ASO choline group was evaluated by ^{1}H NMR through T_1 measurements (considering the behavior of the choline methyl groups, $N^+(CH_3)_3$, at3.2 ppm). T_1 values for the ML_QC and controls are described in Fig. 4 and Table 4.

The T_1 values are associated to the time required for a molecule to reorient along its axis (Bloom and Thewalt, 1994). Thus, T_1 may provide information related to the rotation of a specific lipid region (de

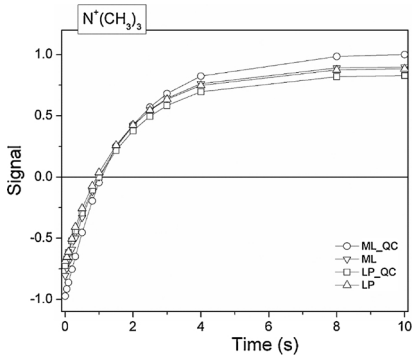

Fig. 4. QC effect on the recovery of asolectin magnetoliposomes (ML) and liposomes (LP) and ^{1}H FID signal after several inversion pulses, related to choline ($N^+(CH_3)_3$) group (3.2 ppm). The circle curves are related to QC-loaded magnetoliposomes (ML_QC), inverted triangle curves to magnetoliposomes (ML), square curves to QC-loaded liposomes (LP_QC) and triangle curves to liposomes (LP). From these curves, the NMR ^{1}H longitudinal relaxation time (T_1) values were obtained.

Table 4
Influence of QC on the asolectin magnetoliposomes (ML) and choline liposomes (LP) ($N^+(CH_3)_3$) NMR ^1H spin-lattice relaxation times (T_1).

	$N^+(CH_3)_3$NMR ^1H T_1(s)
ML_QC	1.86 ± 0.03
ML	1.58 ± 0.06
LP_QC	1.61 ± 0.04
LP	1.57 ± 0.05

The values are shown as the mean ± standard deviation for each group (n = 3).

Sousa et al., 2013). Compared to the ML, the ML_QC showed a 18% higher choline T_1value. The variation of 0.28 s between the referred values suggests a more restricted rotation in ML_QC choline group than in ML (Lepore et al., 1992; Brainard and Cordes, 1981). In contrast, QC did not significantly change the choline $T_1$of the LPs, compared to LP_QC. This suggests that the QC/MNP complex affects the rotation of lipid polar choline region (see Sections 3.1 and 3.3).

The hydration state of lipid phosphate group may be monitored by the analysis of frequency and bandwidth of HATR-FTIR ν_{as} PO_2^- peak (Table 3) (Lee and Chapman, 1986; Garcia et al., 1993). A shift in HATR-FTIR ν_{as} PO_2^- frequency value indicates a change in the number and orientation of hydrogen bonds (provided by water or an active substance) around the phosphate head group (Toyran and Severcan, 2003).

Thus, with respect to the QC influence on the ML lipid phosphate group, HATR-FTIR ν_{as} PO_2^- frequency analyses showed no QC-induced changes in the number of hydrogen-bounded water molecules around the ML lipid phosphate (Garcia et al., 1993). Conversely, the control LP_QC showed a ν_{as} PO_2^- frequency 5.79 cm^{-1} higher than LP. QC significantly affected the hydration degree of the LP phosphate group, increasing the number of hydrogen bonds in the phosphate polar region (Manrique-Moreno et al., 2011b). The enhancement of the hydration degree of LP phosphate may be justified by its interaction with QC hydroxyl groups. Indeed, the QC 3′,4′ hydroxyl groups of ring B, as well as those in position 7 of ring A may interact with LP phosphate by water bridges (Sinha et al., 2011). Hydrogen bonds involving a QC keto group and LP oxygen group may also be responsible for this behavior (Cieslik-Boczula et al., 2012). Since this interaction did not occur in the ML_QC, the QC-induced reorientation of the ML choline group above the phosphate plane may be related to the presence of QC/MNP complex, which interferes in the QC-polar lipid head interaction (Zafar et al., 2014; Tarahovsky et al., 2012).

Bandwidth variations related to a specific lipid stretching band are affected by vibrational, rotational and translational effects, or conformational changes in a lipid region (Toyran and Severcan, 2003). No variation related the ML_QC and ML HATR-FTIR bandwidth values (Table 3) was observed. Thus, QC showed no influence in the phosphate conformation of ML. LP_QC ν_{as} PO_2^- bandwidth analyses showed a 1.67 cm^{-1}smaller value, compared to LP. Thus, QC seems to discreetly restrict LP phosphate mobility. This behavior was observed by Pawlikowska-Pawlega et al. (2014) in studies related to dipalmitoyl-PC membranes.

^{31}P NMR experiments were performed to obtain data concerning to state-of-phase and rotation parameters of the ML_QC system. The spectra of ML_QC and the ML, LP and LP_QC controls are shown in Fig. 5. All spectra show a high field shoulder and a low field peak, typical of hydrated phospholipids in the inverted hexagonal (H_{II}) phase. The H_{II} phase is related to the PE content in the ASO phospholipid mixture (Rand et al., 1971). Fig. 5 shows that the presence of QC in ML systems (ML_QC) preserved the H_{II} phase. It is known that flavonoid-metal complexes may influence PE phase behavior, according to Kim et al. (2013). In this work, it seems that the MNP concentration was not sufficient to perform a ML or LP phase transition. From the spectra

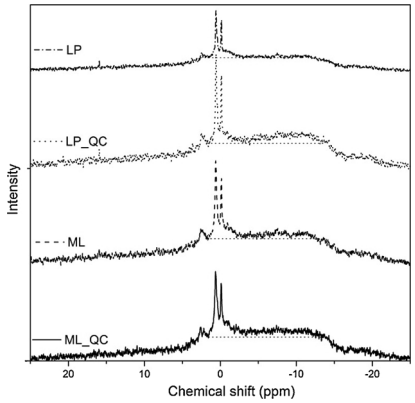

Fig. 5. ^{31}P NMR spectra of QC-loaded magnetoliposomes (ML_QC), magnetoliposomes (ML), QC-loaded liposomes (LP_QC) and liposomes (LP).^{31}P NMR measurements were recorded at 161 MHz, using water/deuterated water (70:30, v/v) as solvent the reference.

Table 5
Influence of QC on the NMR ^{31}Pline width of asolectin magnetoliposomes (ML) and liposomes (LP).

	NMR ^{31}P line width (ppm)
ML_QC	18.14 ± 0.50
ML	16.58 ± 0.36
LP_QC	16.90 ± 0.42
LP	15.17 ± 0.39

The values are shown as the mean ± standard deviation for each group (n = 3).

shown in Fig. 5, line width values are described in Table 5.

ML_QC showed a 9.4% higher line width ^{31}P NMR peak compared to ML. A similar behavior was observed in LP, after interacting with the flavonoid (where an increase of 11.4% in the LP_QC line width was observed). Thus, results indicate that QC decreases the rotational freedom related to the ML and LP phosphate groups. Studies regarding the interaction between apigenin and DPPC membrane associate a flavonoid-induced lipid polar head rigidifying effect with the formation of hydrogen bonds (Pawlikowska-Pawlega et al., 2013). Thus, in the absence of QC-phosphate hydrogen bonds in ML_QC, the ordering effect of QC may be due to a physical interaction between MNP and the flavonoid (QC/MNP complex) (Kim et al., 2013).

3.4.2. QC effects in ML carbonyl region

Variations in HATR-FTIR ν C═O peaks reflect change in carbonyl hydration state and polarity (Severcan et al., 2005). Thus, since no QC-induced changes in ML ν C═O frequency was detected (Table 3), the flavonoid did not affected the number of hydrogen bonds in the lipid carbonyl region.

HATR-FTIR results (Fig. 3 and Table 3) show that ML_QC sample has the ν C═O (at around 1734 cm^{-1}) bandwidth 3.56 cm^{-1} higher than that detected for ML. This indicates that ML_QC has a higher disorder degree in the carbonyl region. A similar behavior was observed for the LP_QC control, compared to the LP control. The QC disorder in LP bilayers, and probably in ML ones, is attributed to the planar flavonoid conformation (Saija et al., 1995). The conformation of QC molecules may be responsible for the disorder of phospholipid carbonyl region by promoting the kink-like acyl conformations near these regions (Movileanu et al., 2000).

3.4.3. QC effects in methylenes of ML hydrophobic chains

The HATR-FTIR results described in Fig. 3 and Table 3 show that QC did not cause variation in the ν CH_2 frequencies and bandwidths. This indicates that there was not a QC-induced change in the trans-gauche

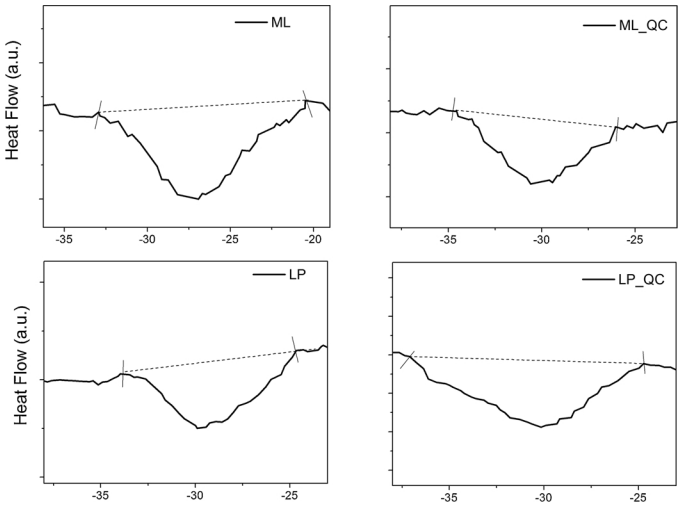

Fig. 6. Zoom of DSC curves of QC-loaded magnetoliposomes (ML_QC), magnetoliposomes (ML), QC-loaded liposomes (LP_QC) and liposomes (LP). In each DSC experiment, the heating rate was set to 5 °C, and the temperature ranged from −40 to 5 °C, under nitrogen flow (50/50 mL min^{-1}). The total QC to ASO ratio was 0.0015 w/w; equivalent to a QC concentration of 500 μmol L^{-1}, and the ASO concentration was 100 mg mL^{-1}.

isomerization of the ML methylenes (Manrique-Moreno et al., 2010).

To obtain information concerning the thermodynamic behavior of the ML_QC, the system phase transition temperature (T_m) and ΔH were studied by the DSC technique and compared with control data. The thermodynamic parameters of the ASO acyl chain methylenes are sensitive to phase transitions, exogenous substances and changes in the chain organization (Lee and Chapman, 1986).

Fig. 6 shows DSC curves related to the ML_QC, ML and the respective LP_QC and LP controls. All curves show an endothermic transition ranging from −40 to −18 °C due to the T_m of the ASO oleic acid (around −20 °C) (Koynova and Caffrey, 2001). From Fig. 6, T_m and ΔH were calculated and listed in Table 6. The ML_QC showed a reduction of $|3.66|$ °C and 0.12 J g^{-1} in T_m and ΔH values, respectively, when compared to the ML values. These results suggest a QC-induced ML hydrophobic chain rearrangement to a less ordered state.

From Table 6, one can also observe that QC did not alter the thermodynamic parameters of the LP acyl chain methylenes. Thus, comparing the LP and ML results, the insertion of MNP into membranes shifts T_m by around 3 °C toward higher values, reflecting an ordering effect. However, after the insertion of QC in this system (i.e. the ML_QC system), an interaction and intercalation of QC and MNP in the lipid head and carbonyl regions may be responsible for reducing the communication of lipid methylenes, acting as spacers between them. This may cause the lipid mosaic destabilization, justifying the disordering effect in the hydrophobic region of the ML_QC (Saija et al., 1995). This hypothesis may be reinforced by the fact that, as shown in Table 6, the insertion of QC did not induce a significant ΔH variation in both ML and LP systems. Unsaturated lipidic systems show a highly cooperative endothermic transition at negative temperatures (Marin et al., 2018). Lipid ΔH is influenced by the unsaturation position related to the geometric center of the hydrocarbon chain. Thus, ΔH values are associated to the degree of interdigitation, presence and number of cis double bonds, which influences the molecular packing of the lipid bilayer. Considering $T_m = \Delta H^\circ/\Delta S^\circ$, ΔH-related stability variation may be associated to a local perturbation of van der Waals chain-chain interaction (Koynova and Caffrey, 2001). In this work, QC did not seem to perturb van der Walls interactions between asolectin acyl chains.

The lipid methylenes T_1 relaxation parameter is sensitive to trans-gauche methylene isomerizations (Deese et al., 1982). Thus, NMR ^1H T_1 measurements of ML_QC acyl chain methylenes were performed to investigate if, as expected according to DSC responses, QC induced the ML hydrophobic region bond rotation rate (Kroon et al., 1976). Fig. 7 shows the recovery of the ML_QC acyl chain methylenes ^1H (at 1–2 ppm) FID as well as the curves related to the ML and LP control samples. Their calculated T_1 values are shown in Table 7. From Table 7, one can see that the ML_QC system showed a 0.98 s lower T_1 value and an enhanced rotation rate, compared to the related ML value. In contrast, QC did not induce changes in LP methylenes T_1. Thus, the enhancement in the QC-induced ML methylene rotation rate may support the hypothesis of the flavonoid-induced reduction of the intermolecular interaction of methylenes proposed in the discussion of the DSC results.

From molecular dynamic studies, it was possible to verify that QC interacts with the lipid head and carbonyl regions of ML, affecting the hydrophobic region. The QC induced a restriction in ML lipid head and disorders, by acting as a spacer, the carbonyl and methylene regions. A schematic illustration of the interaction among QC and lipid molecules and MNP in ML_QC samples is shown in Fig. 8.

Table 6
Influence of QC on the asolectin magnetoliposomes (ML) and liposomes (LP) in enthalpy variation (ΔH) and temperature phase transition (T_m) values.

	T_m (°C)	ΔT_m	ΔH (J g^{-1})	$\Delta\Delta H$
ML_QC	−30.59 ± 0.98		0.16 ± 0.02	
ML	−26.93 ± 1.13	3.66	0.28 ± 0.03	0.12
LP_QC	−29.96 ± 1.06		0.16 ± 0.02	
LP	−29.98 ± 0.95	0.02	0.19 ± 0.02	0.03

The values are shown as the mean ± standard deviation for each group (n = 3).

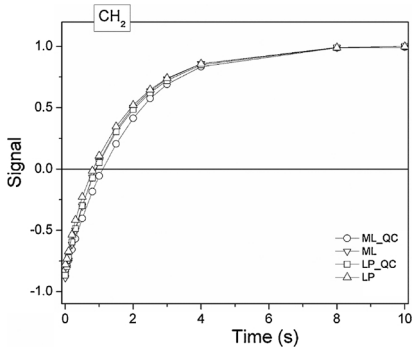

Fig. 7. The QC effect on the recovery of the asolectin liposomes and magnetoliposomes ^1H FID signals after several inversion pulses. Relaxation time of NMR ^1H T_1acyl chain methylenes (CH_2). The circle curves are related to the QC-loaded magnetoliposomes (ML_QC), inverted triangle curves to magnetoliposomes (ML), square curves to QC-loaded liposomes (LP_QC) and triangle curves to liposomes (LP). From these curves, the NMR ^1H longitudinal relaxation time (T_1) values were obtained.

Table 7
Influence of QC on the asolectin magnetoliposomes (ML) and asolectin liposomes (LP) in the relaxation time of NMR T_1 ^1H CH_2.

	NMR ^1H T_1CH_2 (s)	Δ
ML_QC	0.48 ± 0.03	
ML	1.46 ± 0.09	0.98
LP_QC	1.50 ± 0.08	
LP	1.43 ± 0.03	0.07

The values are shown as the mean ± standard deviation for each group (n = 3).

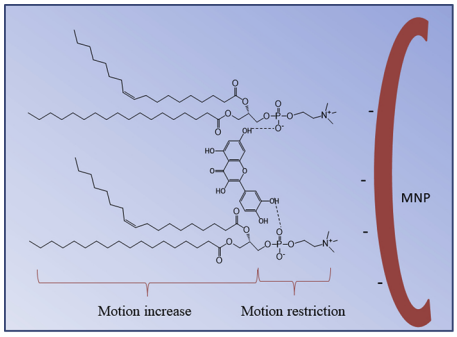

ML_QC

Fig. 8. Schematic representation of molecular interaction among QC, lipid molecules and MNP in the ML_QC system.

3.5. ML_QC oxidation profile

Table 8 reports the amount of TBARS (in μmol TBARS mg^{-1} lipid) produced in basal lipoperoxidation (oxidation caused by atmospheric reactive species) of ML_QC and ML, comparing them with data related to their LP_QC and LP controls. According to Table 6, comparing ML and LP values, the presence of MNP enhances the membrane lipid peroxidation by 3 times. Thus, MNP contributes significantly to the oxidation process of ML. However, ML_QC oxidation is prevented by 8 times against lipid peroxidation compared to ML. QC is then able to inhibit 88% of the ML basal lipid peroxidation process. In contrast, with the same concentration, QC inhibited 36% of the LP basal peroxidation. This means it is probable that QC/MNP interaction has an important role in the stability of ML_QC systems.

Gabrielska et al. (2006) showed that QC reduced the pro-oxidant action of organometallic compounds on membranes of UV irradiated PC liposomes. One of the antioxidant mechanisms of QC is the chelation of metallic ions, such as Cu (II) and Fe (II), preventing free radical formation (RiceEvans et al., 1997; Pietta, 2000). In this case, QC B(3′ and 4′-hydroxyl groups, catechol groups) and C(3-hydroxyl-4-carbonyl and 5-hydroxyl-4-carbonyl groups) rings are responsible for the metal chelating ability of quercetin (Tarahovsky et al., 2014). The preferred site of chelation is located on the 3-hydroxyl-4-carbonyl group, being that iron can produce complexes with one, two or three molecules of quercetin (Ren et al., 2008). Fig. 9 illustrates a purpose of QC antioxidant action in ML_QC via ring C metal chelation.

Table 8
Amount of TBARS produced after basal lipid peroxidation of the ML_QC and ML, LP_QC and LP controls.

	μmol MDA mg^{-1} lipid	% of lipid peroxidation
ML_QC	0.0067 ± 0.002	12.43
ML	0.0539 ± 0.008	100
LP_QC	0.0103 ± 0.002	64.78
LP	0.0159 ± 0.004	100

The values are shown as the mean ± standard deviation for each group (n = 3).

3.6. Cell viability of the ML_QC system

The effect of QC-loaded magnetoliposomes (ML_QC) and the ML, MNP, LP_QC and LP controls on the C6cell viability was investigated and is shown in Fig. 10. The ML_QC decreased C6 cell viability by 44.93%. Compared to ML activity, which reduced cell viability by 33.88%, the ML_QC were 11% more active against C6 cells. ML_QC and ML were 16% and 5% more efficient than the MNP control. Also, LP_QC were 12% more efficient against C6 than the correspondent LP (reduced by 38.77% and 26.12% C6 cell viability, respectively). Thus, the QC effect in C6 viability is similar to ML_QC and LP_QC systems. Wang et al. evaluated the effects of QC PEG2000-DPSE liposomes on C6 glioma cells (Wang et al., 2012). The results demonstrated that QC-liposomes caused necrotic morphological changes and decreased the percentage of viable cells. The high number of hydroxyl groups and conjugated orbitals via which quercetin can donate electrons or hydrogen ions, as well as scavenge H_2O_2 and superoxide anions, make the QC an excellent free radical scavenging antioxidant (Heijnen et al., 2001). It is also possible that the QC hydrophobicity had a considerable role in reducing C6 cell viability, since the MNP insertion into lipid bilayers (ML) did not significantly affect cell mitochondrial respiration (the variation in C6 cell viability after interaction with ML and LP was around 7%). However, it is important to note that no magnetic field was applied in these experiments. The application of an external magnetic force increased MCF-7 and MDA-MB-231 cellular death by artemisin in and transferrin-loaded magnetic liposomes (Gharib et al., 2014). Venugopal et al. evaluated the cytotoxicity of doxorubicin-loaded magnetic nanoparticles on C6 glioma cells (Venugopal et al., 2016). The MTT assay results showed that the glioma cell viability was reduced with exposure to the magnetic field when compared to the no magnetic field exposure (control) group. In contrast, free MNP reduced cell viability by 29.07%, probably by aggregation and oxidative mechanisms in the cells (Yarjanli et al., 2017). It is worth noticing that, without the presence of a magnetic field, the ML_QC was more efficient in reducing C6 viability than the ML, MNP and LP systems, having promising antitumoral activity against glioma cells, with a possible advantage of higher specificity when compared to LP_QC systems.

4. Concluding remarks

In this work, the ML_QC system was characterized physico-chemically and evaluated according to peroxidation susceptibility and C6 cell line toxicity. The system showed 43% of MNP EE%, and superparamagnetic behavior, which is essential for biomedical applications due to the zero magnetization when the applied magnetics field is removed (Kumar et al., 2014). The 200 nm size of the system is appropriate for the parenteral administration. QC and MNP seem to be located at lipid head and carbonyl regions of the system, reorientating the positive-charged choline group to the system surface and ordering the lipid polar head. This is very interesting for the design of dipole attraction-based vectorizing systems, since tumoral cells usually expose negative surface charge.

In contrast, the carbonyl and hydrophobic regions of the ML_QC proved to be disordered, probably because of the intercalating of MNP/QC complexes in the polar head region, which may reduce the intermolecular communication of lipids in carbonyl and non-polar groups. This disorder induced by QC may facilitate the diffusion of drugs which can be inserted in the system, enhancing the delivery rate in cancer therapy. As the QC protected the ML_QC system considerably against peroxidation, the flavonoid may have an important role in system stability. ML_QC reduced C6 cell viability by about 45% without the application of a magnetic field. Thus, ASO-based ML_QC molecular interactions make the many interesting and promising system to be applied in the cancer drug delivery therapy. As far as the authors' know,

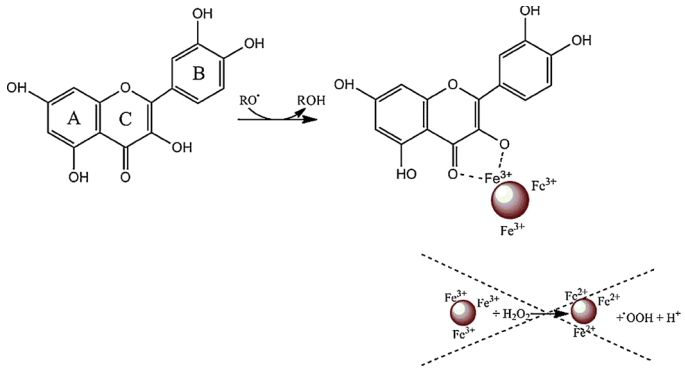

Fig. 9. Illustrative scheme of an antioxidant action of QC when loaded into magnetoliposomes (ML_QC)/QC–Fe complexes.

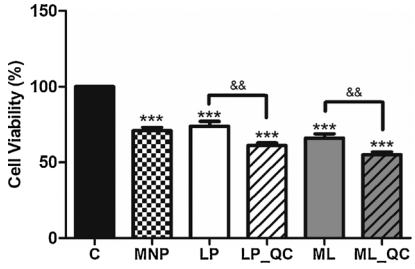

Fig. 10. Cell viability assay in the C6 cell line after 24 h of treatment with magnetoliposomes (ML_QC) and the following controls: free MNP, pure liposomes (LP) or loaded with QC (LP_QC) and magnetoliposomes (ML). Cells were cultured with a concentration of a total QC to ASO ratio was 0.0015 w/w; equivalent to a QC concentration of 500 μmol L^{-1} and a total MNP to ASO ratio was 0.0014 (w/w). n = 5 wells repeated 3 times, ANOVA followed by Tukey-Kramer test. *** $p < 0.001$ (difference from control) && $p < 0.01$ (difference comparing quercetin incorporated into the liposomes or magnetoliposomes and their respective controls). C: control (DMEM only).

the ML_QC molecular interaction approach described in this work is pioneer for the correlation and application of the design for ML-based drug delivery systems.

Acknowledgements

The authors would like to thank the Brazilian agencies Conselho de Desenvolvimento Científico e Tecnológico (CNPq) and Coordenação de Aperfeiçoamento de Pessoal de Nível Superior (CAPES) for their financial support, as well as the Analytical Integrated Center (CIA)-FURG for ^{1}H NMR and ^{31}P NMR analyses. The authors would also like to thank ProfessorJoão Cardoso de Lima, Ph.D. (Laboratory of Material Synthesis and Characterization-LCSM) and the Multiuser Laboratory of Magnetic Characterization of Materials, both from the Physics Department of the Federal University of Santa Catarina, UFSC, SC, Brazil, for the DSC and VSM interpretations. The authors would also like to thank the Hydrochemistry Laboratory from the Institute of Oceanography (FURG) for sample preparations prior to FAAS. This paper is part of Sandra Cruz dos Santos' doctoral thesis, which was carried out in the graduate program of Technological and Environmental Chemistry (FURG).

References

Akal, Z.U., Alpsoy, L., Baykal, A., 2016. Biomedical applications of SPION@APTES@PEG-folic acid@carboxylated quercetin nanodrug on various cancer cells. Appl. Surf. Sci. 378, 572–581.
Babincova, M., Cicmanec, P., Altanerova, V., Altaner, C., Babinec, P., 2002. AC-magnetic field controlled drug release from magnetoliposomes: design of a method for site-specific chemotherapy. Bioelectrochemistry 55, 17–19.
Barenholz, Y., 2001. Liposome application: problems and prospects. Curr. Opin. Colloid Interface Sci. 6, 66–77.
Barreto, A.C.H., Santiago, V.R., Mazzetto, S.E., Denardin, J.C., Lavin, R., Mele, G., Ribeiro, M., Vieira, I.G.P., Goncalves, T., Ricardo, N., Fechine, P.B.A., 2011. Magnetic nanoparticles for a new drug delivery system to control quercetin releasing for cancer chemotherapy. J. Nanopart. Res. 13, 6545–6553.
Berkowitz, A.E., Lahut, J.A., Vanburen, C.E., 1980. Properties of magnetic fluid particles. IEEE Trans. Magn. 16, 184–190.
Bird, R.P., Draper, H.H., 1984. Comparative studies on different methods of malonaldehyde determination. Meth. Enzymol. 105, 299–305.
Bixner, O., Reimhult, E., 2016. Controlled magnetosomes: embedding of magnetic nanoparticles into membranes of monodisperse lipid vesicles. J. Colloid Interface Sci. 466, 62–71.
Bloom, M., Thewalt, J., 1994. Spectroscopic determination of lipid dynamics in membranes. Chem. Phys. Lipids 73, 27–38.
Brainard, J.R., Cordes, E.H., 1981. C-13 nuclear-resonance studies of cholesterol egg-yolk phosphatidylcholine vesicles. Biochemistry 20, 4607–4617.
Budhian, A., Siegel, S.J., Winey, K.I., 2007. Haloperidol-loaded PLGA nanoparticles: systematic study of particle size and drug content. Int. J. Pharm. 336, 367–375.
Caddeo, C., Pons, R., Carbone, C., Fernandez-Busquets, X., Cardia, M.C., Maccioni, A.M., Fadda, A.M., Manconi, M., 2017. Physico-chemical characterization of succinyl chitosan-stabilized liposomes for the oral co-delivery of quercetin and resveratrol. Carbohydr. Polym. 157, 1853–1861.
Chakraborty, S., Stalin, S., Das, N., Choudhury, S.T., Ghosh, S., Swarnakar, S., 2012. The use of nano-quercetin to arrest mitochondrial damage and MMP-9 upregulation during prevention of gastric inflammation induced by ethanol in rat. Biomaterials 33, 2991–3001.
Chen, C., Tripp, C.P., 2008. An infrared spectroscopic based method to measure membrane permeance in liposomes. Biochim. Biophys. Acta Biomembr. 1778, 2266–2272.
Chen, Y., Bose, A., Bothun, G.D., 2010. Controlled release from bilayer-decorated magnetoliposomes via electromagnetic heating. ACS Nano 4, 3215–3221.
Cieslik-Boczula, K., Maniewska, J., Grynkiewicz, G., Szeja, W., Koll, A., Hendrich, A.B., 2012. Interaction of quercetin, genistein and its derivatives with lipid bilayers—an ATR IR-spectroscopic study. Vib. Spectrosc. 62, 64–69.
da Silva, G.B., Marciello, M., Morales, M.D., Serna, C.J., Vargas, M.D., Ronconi, C.M., Costo, R., 2017. Studies of the colloidal properties of superparamagnetic iron oxide nanoparticles functionalized with platinum complexes in aqueous and PBS Buffer Media. J. Braz. Chem. Soc. 28, 731–739.
da Silveira, E.F., Chassot, J.M., Teixeira, F.C., Azambuja, J.H., Debom, G., Beira, F.T., Del Pino, F.A.B., Lourenco, A., Horn, A.P., Cruz, L., Spanevello, R.M., Braganhol, E., 2013. Ketoprofen-loaded polymeric nanocapsules selectively inhibit cancer cell growth in vitro and in preclinical model of glioblastoma multiforme. Invest. New Drugs 31, 1424–1435.
de Lima, V.R., Caro, M.S.B., Munford, M.L., Desbat, B., Dufourc, E., Pasa, A.A., Creczynski-Pasa, T.B., 2010. Influence of melatonin on the order of phosphatidylcholine-based membranes. J. Pineal Res. 49, 169–175.
de Sousa, R.S., Nogueira, A.O.D., Marques, V.G., Clementin, R.M., de Lima, V.R., 2013. Effects of alpha-eleostearic acid on asolectin liposomes dynamics: relevance to its antioxidant activity. Bioorg. Chem. 51, 8–15.
Deese, A.J., Dratz, E.A., Hymel, L., Fleischer, S., 1982. Proton NMR T1, T2, and T1-RHO relaxation studies of native and reconstituted sarcoplasmic-reticulum and phospholipid-vesicles. Biophys. J. 37, 207–216.
Ding, X.W., Cai, K.Y., Luo, Z., Li, J.H., Hu, Y., Shen, X.K., 2012. Biocompatible magnetic liposomes for temperature triggered drug delivery. Nanoscale 4, 6289–6292.
dos Santos, M.C., Kroetz, T., Dora, C.L., Giacomelli, F.C., Frizon, T.E.A., Pich, C.T., Pinto, L.D., Soares, A.S., Rodembusch, F.S., de Lima, V.R., Dal-Bo, A.G., 2018. Elucidating Bauhinia variegata lectin/phosphatidylcholine interactions in lectin-containing liposomes. J. Colloid Interface Sci. 519, 232–241.
Dresco, P.A., Zaitsev, V.S., Gambino, R.J., Chu, B., 1999. Preparation and properties of magnetite and polymer magnetite nanoparticles. Langmuir 15, 1945–1951.
Edwards, K.A., Baeumner, A.J., 2006. Analysis of liposomes. Talanta 68, 1432–1441.
Fagali, N., Catala, A., 2009. Fe2+ and Fe3+ initiated peroxidation of sonicated and non-sonicated liposomes made of retinal lipids in different aqueous media. Chem. Phys. Lipids 159, 88–94.
Floris, A., Sinico, C., Fadda, A.M., Lai, F., Marongiu, F., Scano, A., Pilloni, M., Angius, F., Vazquez-Vazquez, C., Ennas, G., 2014. Characterization and cytotoxicity studies on liposome-hydrophobic magnetite hybrid colloids. J. Colloid Interface Sci. 425,

118–127.
Gabrielska, J., Soczynska-Kordala, M., Hladyszowski, J., Zylka, R., Miskiewicz, J., Przestalski, S., 2006. Antioxidative effect of quercetin and its equimolar mixtures with phenyltin compounds on liposome membranes. J. Agric. Food Chem. 54, 7735–7746.
Garcia, F.L., Micol, V., Villalain, J., Fernandez, J.C.G., 1993. Infrared spectroscopic study of the interaction of diacylglycerol with phosphstidylserine in the presence of calcium. Biochim. Biophys. Acta 1169, 264–272.
Gharib, A., Faezizadeh, Z., Mesbah-Namin, S.A.R., Saravani, R., 2014. Preparation, characterization and in vitro efficacy of magnetic nanoliposomes containing the artemisinin and transferrin. DARU—J. Pharm. Sci. 22, 44–51.
Grdadolnik, J., Kidric, J., Hadzi, D., 1991. Hydratation of phosphatidylcholine reverse micelles and multilayers - An infrared spectroscopic study. Chem. Phys. Lipids 59, 57–68.
Guo, H., Chen, W., Sun, X., Liu, Y.-N., Li, J., Wang, J., 2015. Theranostic magnetoliposomes coated by carboxymethyl dextran with controlled release by low-frequency alternating magnetic field. Carbohydr. Polym. 118, 209–217.
Guo, Y., Zhang, Y., Ma, J., Li, Q., Li, Y., Zhou, X., Zhao, D., Song, H., Chen, Q., Zhu, X., 2018. Light/magnetic hyperthermia triggered drug released from multifunctional thermo-sensitive magnetoliposomes for precise cancer synergetic theranostics. J. Control. Release 272, 145–158.
Gutteridge, J.M.C., 1995. Lipid-peroxidation and antioxidants as biomarkers of tissue-damage. Clin. Chem. 41, 1819–1828.
Hadrich, G., Monteiro, S.O., Rodrigues, M.R., de Lima, V.R., Putaux, J.L., Bidone, J., Teixeira, H.F., Muccillo-Baisch, A.L., Dora, C.L., 2016. Lipid-based nanocarrier for quercetin delivery: system characterization and molecular interactions studies. Drug Dev. Ind. Pharm. 42, 1165–1173.
Hardiansyah, A., Yang, M.C., Liu, T.Y., Kuo, C.Y., Huang, L.Y., Chan, T.Y., 2017. Hydrophobic drug-loaded pegylated magnetic liposomes for drug-controlled release. Nanoscale Res. Lett. 12.
Heijnen, C.G.M., Haenen, G., van Acker, F.A.A., van der Vijgh, W.J.F., Bast, A., 2001. Flavonoids as peroxynitrite scavengers: the role of the hydroxyl groups. Toxicol. In Vitro 15, 3–6.
Hirpara, K.V., Aggarwal, P., Mukherjee, A.J., Joshi, N., Burman, A.C., 2009. Quercetin and its derivatives: synthesis, pharmacological uses with special emphasis on anti-tumor properties and prodrug with enhanced bio-availability. Anticancer Agents Med. Chem. 9, 138–161.
Hollman, P.C.H., vanderGaag, M., Mengelers, M.J.B., vanTrijp, J.M.P., deVries, J.H., Katan, M.B., 1996. Absorption and disposition kinetics of the dietary antioxidant quercetin in man. Free Radic. Biol. Med. 21, 703–707.
Honary, S., Zahir, F., 2013. Effect of zeta potential on the properties of nano-drug delivery systems—a review (Part 2). Trop. J. Pharm. Res. 12, 265–273.
Huang, M.G., Su, E.Z., Zheng, F.P., Tan, C., 2017. Encapsulation of flavonoids in liposomal delivery systems: the case of quercetin, kaempferol and luteolin. Food Funct. 8, 3198–3208.
Jangde, R., Singh, D., 2016. Preparation and optimization of quercetin-loaded liposomes for wound healing, using response surface methodology. Artif. Cells Nanomed. Biotechnol. 44, 635–641.
Jeon, S., Yoo, C.Y., Park, S.N., 2015. Improved stability and skin permeability of sodium hyaluronate-chitosan multilayered liposomes by layer-by-layer electrostatic deposition for quercetin delivery. Colloids Surf. B: Biointerfaces 129, 7–14.
Johns, A., Morris, S., Edwards, K., Quirino, R.L., 2015. Asolectin from soybeans as a natural compatibilizer for cellulose-reinforced biocomposites from tung oil. J. Appl. Polym. Sci. 132, 41833–41842.
Khaleghi, S., Rahbarizadeh, F., Ahmadvand, D., Malek, M., Hosseini, H.R.M., 2016. The effect of superparamagnetic iron oxide nanoparticles surface engineering on relaxivity of magnetoliposome. Contrast Media Mol. Imaging 11, 340–349.
Kim, Y.A., Tarahovsky, Y.S., Yagolnik, E.A., Kuznetsova, S.M., Muzafarov, E.N., 2013. Lipophilicity of flavonoid complexes with iron(II) and their interaction with liposomes. Biochem. Biophys. Res. Commun. 431, 680–685.
Kiwada, H., Sato, J., Yamada, S., Kato, Y., 1986. Feasibility of magnetic liposomes as a targeting debice for drugs. Chem. Pharm. Bull. 34, 4253–4258.
Koynova, R., Caffrey, M., 2001. Phases and phase transitions of the phosphatidylcholines (vol 1376, pg 91, 1998). Biochim. Biophys. Acta Biomembr. 1513, 82.
Kroon, P.A., Kainosho, M., Chan, S.I., 1976. Proton magnetic-resonance studies of lipid bilayr membranes - experimental-determinação of intermolecular and intramolecular nuclear-relaxation rates in sonicated phosphatidylcholine bilayer vesicles. Biochim. Biophys. Acta 433, 282–293.
Kulshrestha, P., Gogoi, M., Bahadur, D., Banerjee, R., 2012. In vitro application of paclitaxel loaded magnetoliposomes for combined chemotherapy and hyperthermia. Colloids Surf. B: Biointerfaces 96, 1–7.
Kumar, S.R., Priyatharshni, S., Babu, V.N., Mangalaraj, D., Viswanathan, C., Kannan, S., Ponpandian, N., 2014. Quercetin conjugated superparamagnetic magnetite nanoparticles for in-vitro analysis of breast cancer cell lines for chemotherapy applications. J. Colloid Interface Sci. 436, 234–242.
Lee, D.C., Chapman, D., 1986. Infrared spectroscopic studies of biomembranes and model membranes. Biosci. Rep. 6, 235–256.
Lepore, L.S., Ellena, J.F., Cafiso, D.S., 1992. Comparison of the lipid acyl chain dynamics between small and large unilamellar vesicles. Biophys. J. 61, 767–775.
Lichtenberg, D., Barenholz, Y., 1988. Liposomes—preparation, characterization and preservation. Methods Biochem. Anal. 33, 337–462.
Lynch, D.V., Steponkus, P.L., 1989. Lyotropic phase-behavior of insaturated phosphatidylcholine species - relevance to the mechanism of plasma-membrane destabilization and freezing-injury. Biochim. Biophys. Acta 984, 267–272.
Makino, K., Yamada, T., Kimura, M., Oka, T., Ohshima, H., Kondo, T., 1991. Temperature-induced and ionic strenght-induced conformational-changes in the lipid head group region of liposomes as suggested by zeta-potential data. Biophys. Chem. 41, 175–183.
Manrique-Moreno, M., Suwalsky, M., Villena, F., Garidel, P., 2010. Effects of the non-steroidal anti-inflammatory drug naproxen on human erythrocytes and on cell membrane molecular models. Biophys. Chem. 147, 53–58.
Manrique-Moreno, M., Garidel, P., Suwalsky, M., Howe, J., Brandenburg, K., 2011a. The membrane-activity of ibuprofen, diclofenac, and naproxen: a physico-chemical study with lecithin phospholipids. Biochim. Biophys. Acta Biomembr. 1808, 1946.
Manrique-Moreno, M., Garidel, P., Suwalsky, M., Howe, J., Brandenburg, K., 2011b. The membrane-activity of ibuprofen, diclofenac, and naproxen: a physico-chemical study with lecithin phospholipids (vol 1788, pg 1296, 2009). Biochim. Biophys. Acta Biomembr. 1808, 1946.
Marie, H., Plassat, V., Lesieur, S., 2013. Magnetic-fluid-loaded liposomes for MR imaging and therapy of cancer. J. Drug Deliv. Sci. Technol. 23, 25–37.
Marin, D., Aleman, A., Montero, P., Gomez-Guillen, M.C., 2018. Encapsulation of food waste compounds in soy phosphatidylcholine liposomes: effect of freeze-drying, storage stability and functional aptitude. J. Food Eng. 223, 132–143.
Martins, M.B.A.F., Corvo, M.L., Marcelino, P., Marinho, H.S., Feio, G., Carvalho, A., 2014. New long circulating magnetoliposomes as contrast agents for detection of ischemia-reperfusion injuries by MRI. Nanomed.—Nanotechnol. Biol. Med. 10, 207–214.
Mertins, O., Sebben, M., Pohlmann, A.R., da Silveira, N.P., 2005. Production of soybean phosphatidylcholine-chitosan nanovesicles by reverse phase evaporation: a step by step study. Chem. Phys. Lipids 138, 29–37.
Movileanu, L., Neagoe, I., Flonta, M.L., 2000. Interaction of the antioxidant flavonoid quercetin with planar lipid bilayers. Int. J. Pharm. 205, 135–146.
Niederberger, W., Seelig, J., 1976. Phosphorus-31 chimical-shift anisotropy in unsonicated phospholipid bilayers. J. Am. Chem. Soc. 98, 3704–3706.
Ohki, S., Muller, M., Arnold, K., Ohshima, H., 2010. Surface potential of phosphoinositide membranes: comparison between theory and experiment. Colloids Surf. B: Biointerfaces 79, 210–218.
Pawlikowska-Pawlega, B., Dziubhiska, H., Krol, E., Trebacz, K., Jarosz-Wilkolazka, A., Paduch, R., Gawron, A., Gruszecki, W.I., 2014. Characteristics of quercetin interactions with liposomal and vacuolar membranes. Biochim. Biophys. Acta Biomembr. 1838, 254–265.
Pawlikowska-Pawlega, B., Misiak, L.E., Zarzyka, B., Paduch, R., Gawron, A., Gruszecki, W.I., 2013. FTIR, 1 H NMR and EPR spectroscopy studies on the interaction of flavone apigenin with dipalmitoylphosphatidylcholine liposomes. Biochim. Biophys. Acta Biomembr. 1828, 518–527.
Pietta, P.G., 2000. Flavonoids as antioxidants. J. Nat. Prod. 63, 1035–1042.
Pradhan, P., Giri, J., Banerjee, R., Bellare, J., Bahadur, D., 2007. Preparation and characterization of manganese ferrite-based magnetic liposomes for hyperthermia treatment of cancer. J. Magn. Magn. Mater. 311, 208–215.
Qiu, D., An, X., Chen, Z., Ma, X., 2012. Microstructure study of liposomes decorated by hydrophobic magnetic nanoparticles. Chem. Phys. Lipids 165, 563–570.
Rand, R.P., Tinker, D.O., Fast, P.G., 1971. Popymorphism of phosphatidylethanolamines from 2 natural sources. Chem. Phys. Lipids 6, 333–342.
Ren, J., Meng, S., Lekka, C.E., Kaxiras, E., 2008. Complexation of flavonoids with iron: structure and optical signatures. J. Phys. Chem. B 112, 1845–1850.
RiceEvans, C.A., Miller, J., Paganga, G., 1997. Antioxidant properties of phenolic compounds. Trends Plant Sci. 2, 152–159.
Saija, A., Bonina, F., Trombetta, D., Tomaino, A., Montenegro, L., Smeriglio, P., Castelli, F., 1995. Flavonoid-biomembrane interactions—a calorimetric study on dipalmitoylphosphatidylcholine vesicles. Int. J. Pharm. 124, 1–8.
Sercombe, L., Veerati, T., Moheimani, F., Wu, S.Y., Sood, A.K., Hua, S., 2015a. Advances and challenges of liposome assisted drug delivery. Front. Pharmacol. 6.
Sercombe, L., Veerati, T., Moheimani, F., Wu, S.Y., Sood, A.K., Hua, S., 2015b. Advances and challenges of liposome assisted drug delivery. Front. Pharmacol. 6, 1–13.
Severcan, F., Sahin, I., Kazanci, N., 2005. Melatonin strongly interacts with zwitterionic model membranes—evidence from Fourier transform infrared spectroscopy and differential scanning calorimetry. Biochim. Biophys. Acta Biomembr. 1668, 215–222.
Shubhra, Q.T.H., Feczko, T., Kardos, A.F., Toth, J., Mackova, H., Horak, D., Dosa, G., Gyenis, J., 2014. Co-encapsulation of human serum albumin and superparamagnetic iron oxide in PLGA nanoparticles: part II. Effect of process variables on protein model drug encapsulation efficiency. J. Microencapsul. 31, 156–165.
Sinha, R., Gadhwal, M.K., Joshi, U.J., SrivaStava, S., Govil, G., 2011. Interaction of quercetin with DPPC model membrane: molecular dynamic simulation, DSC and multinuclear NMR studies. J. Indian Chem. Soc. 88, 1203–1210.
Soenen, S.J.H., Brisson, A.R., De Cuyper, M., 2009. Addressing the problem of cationic lipid-mediated toxicity: the magnetoliposome model. Biomaterials 30, 3691–3701.
Spera, R., Petralito, S., Liberti, M., Merla, C., d'Inzeo, G., Pinto, R., Apollonio, F., 2014. Controlled release from magnetoliposomes aqueous suspensions exposed to a low intensity magnetic field. Bioelectromagnetics 35, 309–312.
Szoka, F., Papahadjopoulos, D., 1978. Procedure for preparation of liposomes with large internal aqueous space and high capture by reverse-phase evaporation. Proc. Natl. Acad. Sci. U. S. A. 75, 4194–4198.
Takagi, T., Takekoshi, S., Okabe, T., Nagata, H., Honma, T., Watanabe, K., 1998. Quercetin, a flavonol, promotes disassembly of microtubules in prostate cancer cells: possible mechanism of its antitumor activity. Acta Histochem. Cytochem. 31, 435–445.
Tarahovsky, Y.S., Yagolnik, E.A., Muzafarov, E.N., Abdrasilov, B.S., Kim, Y.A., 2012. Calcium-dependent aggregation and fusion of phosphatidylcholine liposomes induced by complexes of flavonoids with divalent iron. Biochim. Biophys. Acta Biomembr. 1818, 695–702.
Tarahovsky, Y.S., Kim, Y.A., Yagolnik, E.A., Muzafarov, E.N., 2014. Flavonoid-membrane interactions: involvement of flavonoid-metal complexes in raft signaling. Biochim. Biophys. Acta Biomembr. 1838, 1235–1246.

Torchilin, V.P., 2005. Recent advances with liposomes as pharmaceutical carriers. Nat. Rev. Drug Discov. 4, 145–160.
Toyran, N., Severcan, F., 2007. Interaction between vitamin D-2 and magnesium in liposomes: differential scanning calorimetry and FTIR spectroscopy studies. J. Mol. Struct. 839, 19–27.
Toyran, N., Severcan, F., 2003. Competitive effect of vitamin D-2 and Ca2+ on phospholipid model membranes: an FTIR study. Chem. Phys. Lipids 123, 165–176.
Ulrich, A.S., Sami, M., Watts, A., 1994. Hydration of DOPC bilayers by differential scanning calorimetry. Biochim. Biophys. Acta Biomembr. 1191, 225–230.
van Hoogevest, P., Wendel, A., 2014. The use of natural and synthetic phospholipids as pharmaceutical excipients. Eur. J. Lipid Sci. Technol. 116, 1088–1107.
Venugopal, I., Pernal, S., Duproz, A., Bentley, J., Engelhard, H., Linninger, A., 2016. Magnetic field-enhanced cellular uptake of doxorubicin loaded magnetic nanoparticles for tumor treatment. Mater. Res. Express 3, 1–13.
Wang, G., Wang, J.J., Yang, G.Y., Du, S.M., Zeng, N., Li, D.S., Li, R.M., Chen, J.Y., Feng, J.B., Yuan, S.H., Ye, F., 2012. Effects of quercetin nanoliposomes on C6 glioma cells through induction of type III programmed cell death. Int. J. Nanomed. 7, 271–280.
Wong, M.Y., Chiu, G.N.C., 2011. Liposome formulation of co-encapsulated vincristine and quercetin enhanced antitumor activity in a trastuzumab-insensitive breast tumor xenograft model. Nanomed. Nanotechnol. Biol. Med. 7, 834–840.
Xia, S.D., Li, P., Chen, Q., Armah, M., Ying, X.Y., Wu, J., Lai, J.T., 2014. In situ precipitation: a novel approach for preparation of iron-oxide magnetoliposomes. Int. J. Nanomedicine 9, 2607–2617.
Yarjanli, Z., Ghaedi, K., Esmaeili, A., Rahgozar, S., Zarrabi, A., 2017. Iron oxide nanoparticles may damage to the neural tissue through iron accumulation, oxidative stress, and protein aggregation. BMC Neurosci. 18, 51–63.
Ye, H., Tong, J.S., Liu, J.Y., Lin, W.M., Zhang, C.S., Chen, K., Zhao, J., Zhu, W.J., 2016. Combination of gemcitabine-containing magnetoliposome and oxaliplatin-containing magnetoliposome in breast cancer treatment: a possible mechanism with potential for clinical application. Oncotarget 7, 43762–43778.
Zafar, N., Fessi, H., Elaissari, A., 2014. Cyclodextrin containing biodegradable particles: from preparation to drug delivery applications. Int. J. Pharm. 461, 351–366.
Zhao, L., Feng, S.-S., Kocherginsky, N., Kostetski, I., 2007a. DSC and EPR investigations on effects of cholesterol component on molecular interactions between paclitaxel and phospholipid within lipid bilayer membrane. Int. J. Pharm. 338, 258–266.
Zhao, H., Gagnon, J., Häfeli, U.O., 2007b. Process and formulation variables in the preparation of injectable and biodegradable magnetic microspheres. Biomagn. Res. Technol. 5, 1–11.